The Astrophysical Journal Supplement Series, 216:1 (10pp), 2015 January doi:10.1088/0067-0049/216/1/1

NEW Fe I LEVEL ENERGIES AND LINE IDENTIFICATIONS FROM STELLAR SPECTRA

Ruth C. Peterson[1] and Robert L. Kurucz[2]
[1] SETI Institute and Astrophysical Advances, 607 Marion Place, Palo Alto, CA 94301, USA; peterson@ucolick.org
[2] Harvard-Smithsonian Center for Astrophysics, 60 Garden Street, Cambridge, MA 02138, USA
Received 2014 June 3; accepted 2014 October 30; published 2014 December 15

ABSTRACT

The spectrum of the Fe I atom is critical to many areas of astrophysics and beyond. Measurements of the energies of its high-lying levels remain woefully incomplete, however, despite extensive laboratory and solar analysis. In this work, we use high-resolution archival absorption-line ultraviolet and optical spectra of stars whose warm temperatures favor moderate Fe I excitation. We derive the energy for a particular upper level in Kurucz's semiempirical calculations by adopting a trial value that yields the same wavelength for a given line predicted to be about as strong as that of a strong unidentified spectral line observed in the stellar spectra, then checking the new wavelengths of other strong predicted transitions that share the same upper level for coincidence with other strong observed unidentified lines. To date, this analysis has provided the upper energies of 66 Fe I levels. Many new energy levels are higher than those accessible to laboratory experiments; several exceed the Fe I ionization energy. These levels provide new identifications for over 2000 potentially detectable lines. Almost all of the new levels of odd parity include UV lines that were detected but unclassified in laboratory Fe I absorption spectra, providing an external check on the energy values. We motivate and present the procedure, provide the resulting new energy levels and their uncertainties, list all the potentially detectable UV and optical new Fe I line identifications and their *gf* values, point out new lines of astrophysical interest, and discuss the prospects for additional Fe I energy level determinations.

Key words: atomic data – line: identification – methods: laboratory: atomic – stars: individual (HD 29139, HD 72660, HD 76932, HD 85503, HD 94028, HD 124897, HD 140283, HD 157466, HD 160617, HD 165341, HD 184499, HD 211998, HD 217107) – techniques: spectroscopic – ultraviolet: stars

Supporting material: machine-readable table

1. INTRODUCTION

Astrophysical research has dramatically progressed in the last two decades, fueled by rapid advances in key areas. Telescopes and detectors are larger, and make increasingly precise observations of progressively fainter and more distant objects. The analysis of these data sets has surged due to the exponentially increasing capabilities of computers and networked systems.

Lagging far behind are the laboratory astrophysics data necessary to interpret this information. These are the fundamental physical parameters that characterize the spectral absorption and emission of the atomic and molecular systems that pervade stars, stellar nebulae, exploding supernovae, and the interstellar and intergalactic medium, from the local environment to the highest redshifts.

Line parameters for the iron atom are a particularly important case. While energy levels, wavelengths, and transition probabilities (*gf* values) can often be theoretically derived for light, simple atoms, there is no substitute for empirically determining the energy levels of an atom as complex and abundant as iron. Because lines of neutral iron dominate the solar absorption spectrum, especially over 1500 Å–2100 Å where they outnumber Fe II and Si I lines by a factor of five (Tousey 1988), Fe I has been investigated extensively in the laboratory and from the solar spectrum itself.

Summarizing previous work, Nave & Johansson (1993b) derived energies from laboratory spectra for 86 new Fe I levels, from which Nave & Johansson (1993a) identified and established wavelengths for over 2000 Fe I lines from 1700 Å to 5 μm. In the UV, Nave & Johansson (1993b) concluded that "many more solar lines in this region are also due to Fe I, and originate from still higher levels that the ones reported here."

A similar situation prevails in the infrared. To reach Fe I levels with energies from 59000 cm^{-1} to 61700 cm^{-1}, Johansson et al. (1994) and Schoenfeld et al. (1995) analyzed Fe I supermultiplets in the solar infrared spectrum, identifying nearly 200 lines in three IR windows 35, 6, and 40 cm^{-1} wide. These new IR Fe I lines are weak, usually with depths less than 10% of the solar continuum (Johansson et al. 1994, Figure 5). A multitude of unidentified IR lines remain, some of which are strong: Table 6 of Hinkle et al. (1995) lists 72 unidentified lines whose depths are 10% or more in the infrared spectrum of the metal-poor K giant Arcturus (Peterson et al. 1993).

Currently, most of the Fe I lines that remain unidentified fall either in the UV, from 1500 Å to 4000 Å, or in the infrared, beyond 1 μm. Those in the UV are transitions between known low-lying levels to high, still-unmeasured upper levels; those in the infrared are transitions between high levels, one or both of which is unmeasured. Addressing this semiempirically, Kurucz (2011) ran calculations that extrapolate experimentally determined energy values to unknown energy levels and predict the associated wavelengths. His website currently provides results from such comprehensive calculations for all iron-peak elements. However, because wavelengths are fixed by the difference in energy levels, wavelengths of predicted lines are usually in error, typically by 10 Å or more near 2000 Å, and by much more in the infrared.

2. THE NEED FOR NEW Fe I LINE IDENTIFICATIONS

Several areas of astronomy are severely impacted by unidentified Fe I lines. Among these areas are the determinations of

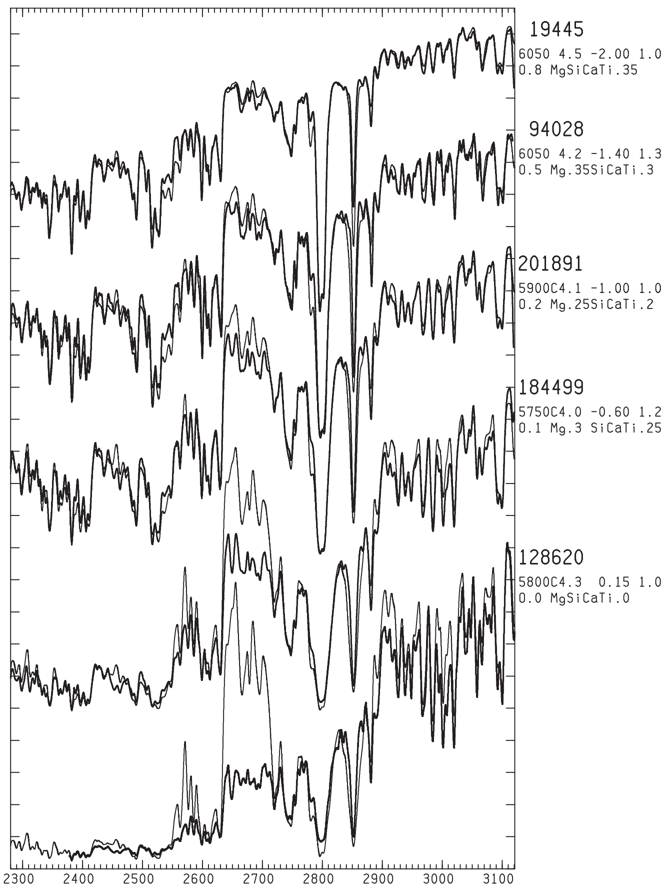

Figure 1. Comparisons are shown of spectral calculations (light lines) to observations (heavy lines) for four metal-poor stars plus α Cen A. Their HD numbers and model parameters appear at the right. Each stellar comparison is vertically offset; Y axis ticks represent 10% of full scale. Wavelengths in Å appear at the bottom. Adapted from Peterson et al. (2002).

abundances for trace elements in individual stars from their UV spectra (e.g., Peterson 2011, 2013), with the potential to unravel the nucleosynthesis processes and environments in which the earliest stars and their heavy elements were formed (Sneden et al. 2008). Identified infrared lines and their *gf* values are vital (Ruffoni et al. 2013) for infrared spectroscopic iron abundances of luminous red giants in dust-obscured regions like the bulge, bar, and disk of the Milky Way plus the Sagittarius stream (Majewski et al. 2010). All across the spectrum, new line identifications are needed to fill significant poorly modeled gaps in spectra of stars of solar metallicity and temperature, improving the fidelity of theoretical models of UV (Peterson et al. 2002) and blue (Coelho 2014) spectral energy distributions (SEDs). These, in turn, are needed to discriminate low metallicity from young age in globular clusters (Dalcanton et al. 2012) and galaxies of moderate redshift (Kelson et al. 2014).

The severity of the problem in the near-UV is seen in Figure 1, adapted from Peterson et al. (2002). This compares observed spectra of five near-turnoff stars whose metallicities range from 1/100 solar to slightly supersolar ($-2.0 \leqslant$ [Fe/H] $\leqslant +0.15$). Observed stellar near-UV fluxes (heavy lines) are superimposed on theoretical spectra (light lines) that Peterson et al. (2001) calculated, specifically leaving out the Kurucz predicted lines, whose wavelengths are uncertain. Without them, as temperature drops and metallicity increases, flux is increasingly underestimated in regions not dominated by strong absorption lines. The underestimate reaches a factor of three at solar metallicity in the 2650 Å–2720 Å region, as the light grey lines (the calculations) fall increasingly far above the heavy black lines (the observations). This is unfortunate, because the widely used, high-resolution, 850–4700 Å UVBLUE theoretical spectral templates (Rodriguez-Merino et al. 2005), incorporated into the Koleva & Vazdekis (2012) assessment of the *HST*/STIS Next Generation Spectral Library (Gregg et al. 2006), were also calculated without the Kurucz predicted lines. Below 2300 Å, matters only become worse (Peterson 2011).

3. IDENTIFYING Fe i LINES AND LEVELS FROM STELLAR SPECTRA

To remedy this issue, in our *HST* Cycle 21 AR-13263 program, we have undertaken the identification of these lines in metal-poor turnoff stars directly from their ultraviolet spectra. We first established that unidentified lines are overwhelmingly due to Fe i. This was seen by running calculations over 1600 Å–8900 Å that included only the Kurucz (2011) predicted lines of all neutral species plus Fe ii, covering FGK stars in the temperature range 4000–6500 K. These lines are present in the observed spectra, but have unknown wavelength offsets in the computed spectra.

Peterson then began to empirically establish upper-level energies for Fe i from the same five archival *HST* E230H echelle spectra of Peterson (2011), by matching modified predictions to the positions of their unidentified absorption lines. The procedures are similar to those followed by Castelli & Kurucz (2010) to identify 109 high levels of Fe ii from the optical spectrum of a slowly rotating B star. The energy difference between the upper and lower levels of a transition fixes its wavelength, and in the UV nearly all lower levels have energies found in the laboratory. A trial energy is chosen by shifting the wavenumber for a specific predicted level to match the predicted and observed wavenumbers of a near-UV line that the Kurucz predictions suggest is as strong as an observed but unidentified spectral line. The wavenumbers of the other strong predicted lines that share the same upper level are checked for coincidence with other strong observed unidentified lines. Matching positions exactly and gf values approximately for four or more transitions with same upper level confirms its energy. Other lines of the same multiplet will have similar shifts, so their starting guesses become closer.

A critical aspect of this program is the interplay between new identifications and subsequent predictions. Each new level identification and energy value better constrain the Fe i atomic matrix calculations that produce the predicted lines. Once Peterson has found a number of new levels, Kurucz incorporates these into his computation of the Fe i matrix, described just below. The new energy values strongly constrain levels of similar structure whose energies remain unknown, improving their wavelength predictions for Peterson's next Fe i search.

Predicted energy levels and log *gf* values were computed by Kurucz with his version of the Cowan (1981) code (Kurucz 2009). The calculation included the 61 even configurations $d^6\ 4s^2$, $d^6\ 4s5s$–$10s$, $d^6\ 4s4d$–$10d$, $d^6\ 4s5g$–$9g$, $d^6\ 4s7i$–$9i$, $d^6\ 4s9l$, d^8, $d^7\ 4s$–$10s$, $d^7\ 4d$–$10d$, $d^7\ 5g$–$9g$, $d^7\ 7i$–$9i$, $d^9\ 9l$, $d^5\ 4s^2$, $5s$–$10s$, $d^5\ 4s^2 4d$–$10d$, and $d^6\ 4p^2$ with 18,655 levels least-squares fitted to 447 known levels. The 50 odd configurations included $d^6\ 4s4p$–$9p$, $d^6\ 4s4f$–$9f$, $d^6\ 4s6h$–$9h$, $d^6\ 4s8k$–$9k$, $d^7\ 4p$–$10p$, $d^7\ 4f$–$9f$, $d^7\ 6h$–$9h$, $d^7\ 8k$–$9k$, $d^5\ 4s^2 4p$–$9p$, and $d^5\ 4s^2 4f$–$9f$ with 18,850 levels least-squares fitted to 581 known levels. The calculations were done in LS coupling with all configuration interactions included, with scaled Hartree–Fock

Table 1
Stellar Parameters and Spectra

Star, Model	Wavelength (Å)	Instrument	Program	Reduction	T (ks)
Sun	2960–13000	NSO FTS		Kurucz (2005)	
5775 4.40 +0.00					
HD 29139 (α Tau)	4900–9750	2m NARVAL	U. Heiter	Lebzelter et al. (2012)	
3950 1.10 +0.00		at Pic du Midi			
HD 72660	1630–1902	STIS 230H	GO 9146	Monier	1.65
9525 4.00 +0.35	2129–2888	STIS 230H	GO 9455	StarCat uvsum 52690	1.64
	3022–5845	HIRES	U17H	Prochaska	0.15
HD 76932	1880–2150	STIS 230H	GO 9804	StarCat 53054–53056	23.86
5900 4.10 −1.00	3022–4975	UVES	266.D–5655(A)	Pipeline	0.34
HD 85503 (μ Leo)	5582–5665	HIRES	U44H	Pipeline + IRAF	0.01
4650 2.70 +0.40	5578–8560	HIRES	U63H	Pipeline + IRAF	0.06
HD 94028	1880–2150	STIS 230H	GO 8197	IRAF	33.05
6050 4.30 −1.40	2278–3120	STIS 230M	GO 7402	IRAF	0.60
	3050–4989	UVES	072.B-0585(A)	NGSL	0.75
HD 124897 (Arcturus, α Boo)	3727–9300	Coudé Feed	Hinkle et al.	Hinkle et al. (2000)	
4275 1.30 −0.55		KPNO 0.9m	Table 3		
HD 140283	1950–2300	STIS E230H	GO 7348	StarCat uvsum2126	18.32
5400 3.60 −2.60	2378–2891	STIS E230H	GO 9455	IRAF	5.28
	2885–3147	STIS 230H	GO 9491	StarCat 52831-52844	62.57
	3080–5953	HIRES	U35H	Prochaska	0.60
HD 157466	2378–3158	STIS 230H	GO 9455	IRAF	11.11
6050 4.30 −0.45	3085–3996	HIRES	U35H	Prochaska	1.26
HD 160617	1880–2150	STIS 230H	GO 8197	StarCat 51480-51787	39.39
6000 3.80 −1.80	3057–3873	UVES	65.L-0507(A)	Pipeline	3.00
	4400–6780	HIRES	H6aH	Extracted	0.42
HD 165341	3736–10425	UVES	71.B-0529(A)	Pipeline	0.05
5300 4.50 +0.00					
HD 184499	2378–3159	STIS 230H	GO 9455	IRAF	11.26
5750 4.10 −0.50	3847–4986	HIRES	N01/N12/N13H	Pipeline + IRAF	0.18
HD 211998	1880–2150	STIS 230H	GO 9804	IRAF	29.40
5300 3.30 −2.60	3040–10400	UVES	266.D-5655(A)	Pipeline	0.60
HD 217107	3750–10252	UVES	076.B-0055(A)	Pipeline	0.33
5600 4.20 +0.30	5730–7230	bHROS, Gemini-S	2600A-C-5, 2006B-Q-47	Ghezzi	0.60

starting guesses, and with Hartree–Fock transition integrals. A total of 7512824 lines were saved from the transition array, of which 107602 lines are between known levels and have good wavelengths.

Deriving an energy for a particular Fe I level establishes the identifications and wavelengths for all transitions that share this level and also arise from a known lower level, regardless of its energy and thus its wavelength. Thus a slew of lines from the UV through the IR may be solved in a single level. Because the upper energy remains fixed, the lower energy of this series of transitions increases steadily toward the red. Most of the lower levels of Fe I transitions already have known energies, because these levels are easily populated in laboratory experiments. However, in warm stars at 6000 K, the levels of moderate excitation are more easily detected than in the Brown et al. (1988) ~2000°C iron furnace. The drawback in stars is that many stellar Fe I lines are blended by lines of other elements.

4. STELLAR SPECTRA

Panchromatic stellar spectra are critical to this identification procedure to increase the number of lines for a given level against which a match can be found, since lines that share the same upper level are spread over wavelengths from 1600 Å to 6 μm and beyond. Furthermore, as wavelength increases, line profiles become steadily narrower in wavenumber space, reducing the uncertainty in the deduced energy levels. However, at progressively longer wavelengths, Fe I line strengths are diminished by the lower Boltzmann populations as the lower energy level steadily rises towards the red. Consequently, spectra of progressively stronger-lined stars were adopted at redder wavelengths, culminating in stars of solar-metallicity and higher and solar temperatures or lower as wavelengths approached 1 μm. In the infrared, Nave & Johansson (1993a) note that "the best source for Fe I is the Sun."

Table 1 summarizes the spectra adopted. Below the stellar names are the model parameters $T_{\rm eff}$, log g, and [Fe/H] used for the calculations. The spectral characteristics include the spectrograph, wavelength coverage, the data reduction procedure or the source from which reduced spectra were downloaded, and the exposure times. The sources include StarCat (Ayres 2010**a**), the UVES and HIRES pipelines, and the UVES ground-based spectral programs of the Next Generation Spectral Library (NGSL; Gregg et al. 2006). All spectra are of intrinsically sharp-lined stars (with rotational velocities $v \sin i < 5$ km s^{-1}). Spectral resolution is ~110,000 in the UV and for the solar spectrum, and 100,000 for Arcturus, although turbulence limits the line profiles to an effective resolution of 60,000 to 80,000. Optical spectral resolutions are 50,000–60,000. Signal-to-noise ratios (S/N) exceed 50 for all spectra except below 2000 Å. S/N greatly exceeds this for the best-observed optical spectra, those of the Sun and the metal-poor K giant Arcturus. They were obtained with the Fourier Transform Spectrometer (FTS) and coudé feed spectrograph at Kitt Peak; all the others are echelle grating spectra.

In the optical, we have relied very heavily on the Kurucz (2005) solar flux spectrum and the Hinkle et al. (2000) Arcturus atlas. We were able to disentangle an Fe I line coincident with the Li I doublet thanks to the $R = 140{,}000$, S/N = 750 Gemini-S echelle spectrum of HD 217107 (Ghezzi et al. 2009). We also have made use of the $R = 80{,}000$, S/N > 200 spectrum of the K5 giant α Tau, obtained for the stellar parameter workshop of Lebzelter et al. (2012). The ∼1500 K temperature difference between giants and solar-type stars allows us to better discern the plausible values of the lower excitation potential from the difference in the strength of an unknown line in giants versus solar-type stars. For the ground-based near-UV and blue, we have added archival spectra over a wide metallicity range from VLT/UVES (e.g., Bagnulo et al. 2003) and Keck/HIRES with upgraded UV sensitivity (Vogt et al. 1994). The high quality of the latter and our ability to reproduce them synthetically is seen in the figures of Peterson (2013), who derived abundances for light trans-Fe elements from the 3050–4000Å region of the HIRES spectra of metal-poor dwarfs that Boesgaard et al. (2011) obtained for Be II lines near 3130 Å.

Conversely, progressively more metal-poor stars were included as wavelength decreases. This is essential to reduce line blending, notably the crowding of the unidentified Fe I lines among themselves. Those from odd-parity levels dominate below 2300 Å, and blend so strongly with one another below 1935 Å that Brown et al. (1988) could identify only a handful. To minimize this blending, which is significant even at the lowest stellar metallicities available, we added HD 72660, a metallic-line A star, to isolate the very strongest unidentified Fe I lines. Lines from even-parity levels similarly converge near 2500 Å, since odd-parity levels from which even-parity levels must arise have their lowest energies near 19500 cm^{-1}. This is too high for the furnace of Brown et al., who detected virtually none. In stars of solar temperature, blending is again severe above 1/100 solar metallicity, [Fe/H] = −2.

All but one of the space-based UV spectra were obtained with the E230H echelle grating of the Space Telescope Imaging Spectrograph (STIS). In the mid-UV, for the Hubble Treasury program GO-9455 such spectra were obtained for sharp-lined stars of types sdB, A, F, G, and K at 110,000 resolution out to 3150 Å. Peterson (2008) illustrates how well our calculations match spectra at 3065 Å of the metal-poor turnoff stars HD 184499 and HD 157466, with ($T_{\rm eff}$, log g, [Fe/H]) = (5750 K, 4.1, –0.5) and (6050 K, 4.3, –0.45), as well as the solar-metallicity F5 IV standard Procyon and the Sun itself. The UV spectra near 2000 Å were taken primarily for boron abundances (e.g., Thorén & Edvardsson 2000).

Reliable spectral dispersions and stellar radial velocities are critical to the reliability of the values of the derived Fe I energy levels. The latter were established to 0.05–0.10 km s^{-1} for each individual spectrum by eye, directly from the match of observed and calculated profiles for previously identified Fe I lines of similar lower excitation potential to those expected for unidentified Fe I lines in the same wavelength region. In all cases this absorbs whatever velocity shift is contributed to these lines by stellar convective motions. For the Sun, a shift of 0.25 km s^{-1} was applied, to partially restore the removal of its gravitational redshift from the Kurucz (2005) spectrum. For reference, an 0.1 km s^{-1} shift in velocity corresponds to wavenumber shifts of 0.017 cm^{-1}, 0.008 cm^{-1}, and 0.004 cm^{-1} at air wavelengths of 2000 Å, 4000 Å, and 8000 Å.

The internal reliability of spectral dispersion solutions varies somewhat; bench-mounted FTS and coude feed spectrographs have fewer complications than do echelles on moving platforms and in varying thermal environments (Chaffee & Schroeder 1976). The latter include HIRES, UVES, and STIS. Ayres (2010b) has incorporated improvements in the STIS E230H near-UV echelle dispersion solutions, reducing the three sigma internal error in a given position from 0.3 km s^{-1} for spectra with pipeline reductions to 0.1 km s^{-1} for StarCat spectra. Values typical of the ground-based echelles also fall within this range, judging from the variations in Fe I profile coincidence as well as from overlapping segments of adjacent orders.

5. SPECTRAL SYNTHESIS METHODS

Peterson generates stellar spectra using an updated version of the Kurucz (1993) program SYNTHE. The input is a list of molecular and atomic line transitions with wavelengths, energy levels, and laboratory and computed *gf* values (revised to match the stellar line strengths), and a static, one-dimensional model stellar photosphere of effective temperature $T_{\rm eff}$, gravity log g, overall metallicity [Fe/H], and microturbulent velocity v_t. These parameters are derived exclusively from the spectra, not colors. $T_{\rm eff}$ is derived as noted just below, [Fe/H] from iron lines, and v_t and log g from trends with line strength or ionization, plus the breadth of wings of strong lines. As reported by Peterson et al. (2001), a consistent determination of the stellar temperature emerges from all available diagnostics. These always include demanding the same abundances be deduced from low- and high-excitation lines of the same species, and that the wings of the profiles of Balmer lines be reproduced. If space-based ultraviolet spectra are on hand, we also match mid-UV flux levels and the continuum slope of the mid-UV spectrum. The Balmer wings agree with other $T_{\rm eff}$ diagnostics only when convective overshoot is turned off. We thus use Castelli & Kurucz (2003) ODFNEW models, which also adopt an improved solar iron abundance and continuum and line opacities.

The input line list was improved by comparing calculations to echelle spectra of a wide variety of standard stars. This includes lines identified in the laboratory, but not lines whose wavelengths or identifications are unknown. Moving from weak-lined to stronger-lined stars, each spectrum is calculated, *gf* values are adjusted singly for atomic lines and as a function of band and energy for molecular lines, and both are iterated until all spectra match. These LTE calculations fit both optical and mid-UV spectra of a wide range of metal-poor and solar-metallicity standard stars (Peterson 2005, 2008, 2011, 2013).

Any nonLTE effects are expected to be small for the range in temperature, metallicity, and gravity of the stars considered here (Table 1), according to Lind et al. (2012). Their Figure 2 shows that the nonLTE effect expected on our Fe I abundances never exceeds 0.1 dex. Similarly, from their Figure 6, the nonLTE effect on $T_{\rm eff}$ values derived from Fe I excitation, such as ours, is 30 K or less. Lind et al. (2012) find good agreement between their results and those of Mashonkina et al. (2011); both show smaller nonLTE effects than do previous studies. Lind et al. attribute this to the recent inclusion of the numerous high-lying Fe I levels of the Kurucz (2007) expanded Fe I calculations, providing "a realistic coupling to the next ionization state."

6. ILLUSTRATIONS OF THE LINE IDENTIFICATION PROCEDURE

Figures 2–5 illustrate the identification of a single level via four of its least-blended transitions. Progressing from the ultraviolet redward, each figure includes a line whose upper level is 5.0 (4F)6p 3G, at 59357.03 cm^{-1}. These lines

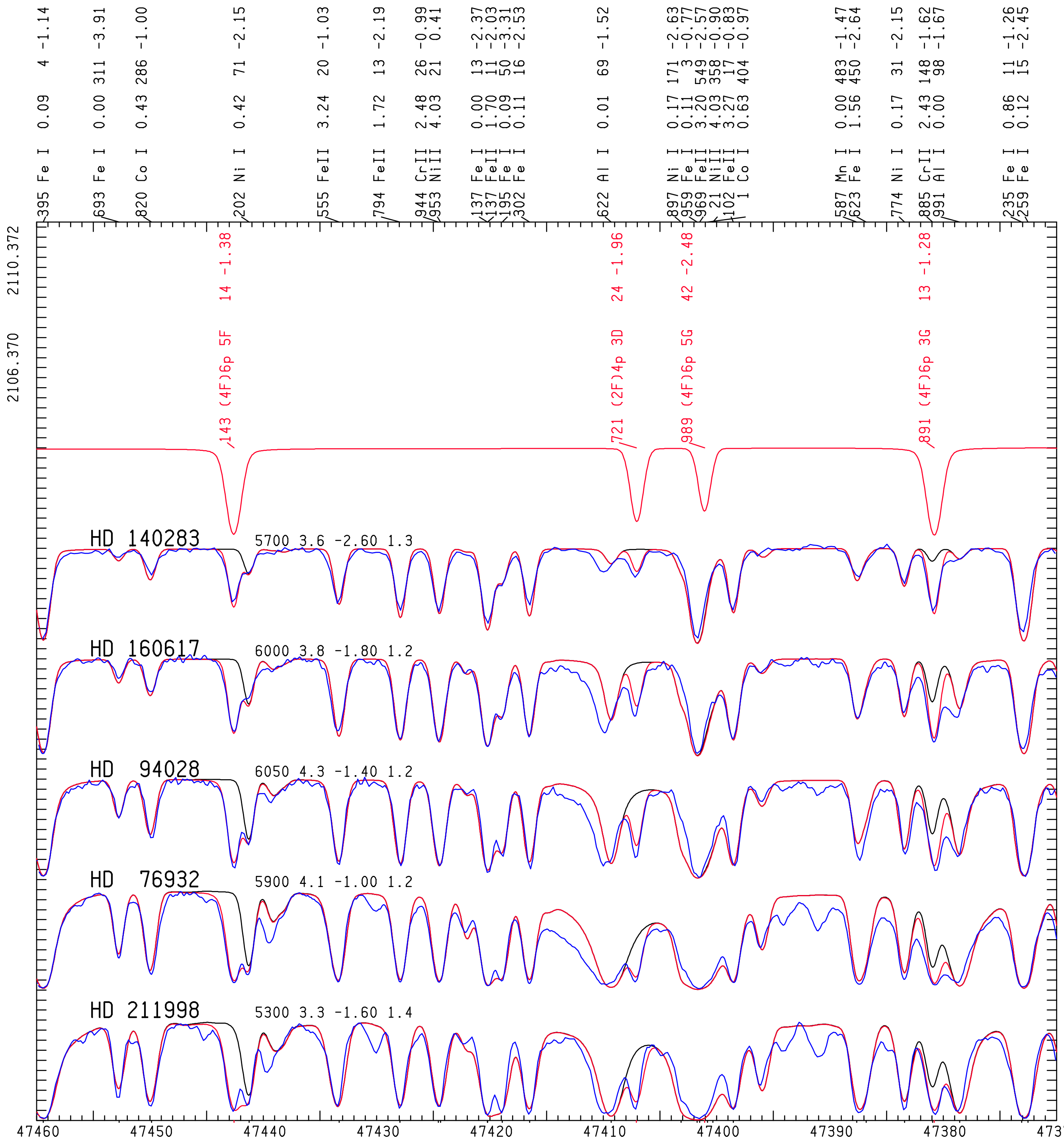

Figure 2. Comparisons are shown in the 2110 Å region between the observed and calculated spectra for five metal-poor stars, vertically offset for clarity. Each tick on the y axis represents one-tenth of full scale. The stellar identification is on the left with the parameters $T_{\rm eff}$, log g, [Fe/H], and v_t, the temperature, gravity, overall metallicity, and microturbulent velocity adopted for the model atmosphere. Wavenumbers in cm^{-1} appear at the bottom. The wavelength range in Å of the plot is given at upper left. Strong lines are identified at the top. First are the digits following the decimal place of the line center wavelength in Å (in air < 2000 Å). Next are the species giving rise to the line, the lower excitation of the line in eV, an indicator of its strength (stronger lines have smaller numbers), and its log *gf* value. Blue lines are observations, which are *HST* STIS spectra below 3050 Å and ground-based in the optical. Black and red lines are spectral calculations. The black line lacks the newly identified Fe I lines; the red line includes them. Only the new lines were included in the top calculation.

are at 47380.79 cm^{-1} (2108.89 Å; Figure 2), 33005.99 cm^{-1} (3028.87 Å; Figure 3), 22311.10 cm^{-1} (4480.82 Å; Figure 4), and 11396.01 cm^{-1} (8772.53 Å, Figure 5). Each plot compares observed and calculated spectra for several stars. Their identifications are given at left, along with the effective temperature $T_{\rm eff}$, gravity log g, metallicity [Fe/H], and microturbulent velocity v_t of the atmospheric model, derived as described above. Observed spectra are in blue. Calculations that include the new line identifications are in red; those lacking them, in black.

The ultraviolet region near 2110 Å in Figure 2 shows four strong newly identified lines and illustrates the high quality of five archival STIS E230H spectra. In Figure 3, the region near 3030 Å shows another four new identifications, all moderately strong. The high S/N HD 140283 spectrum brings out very

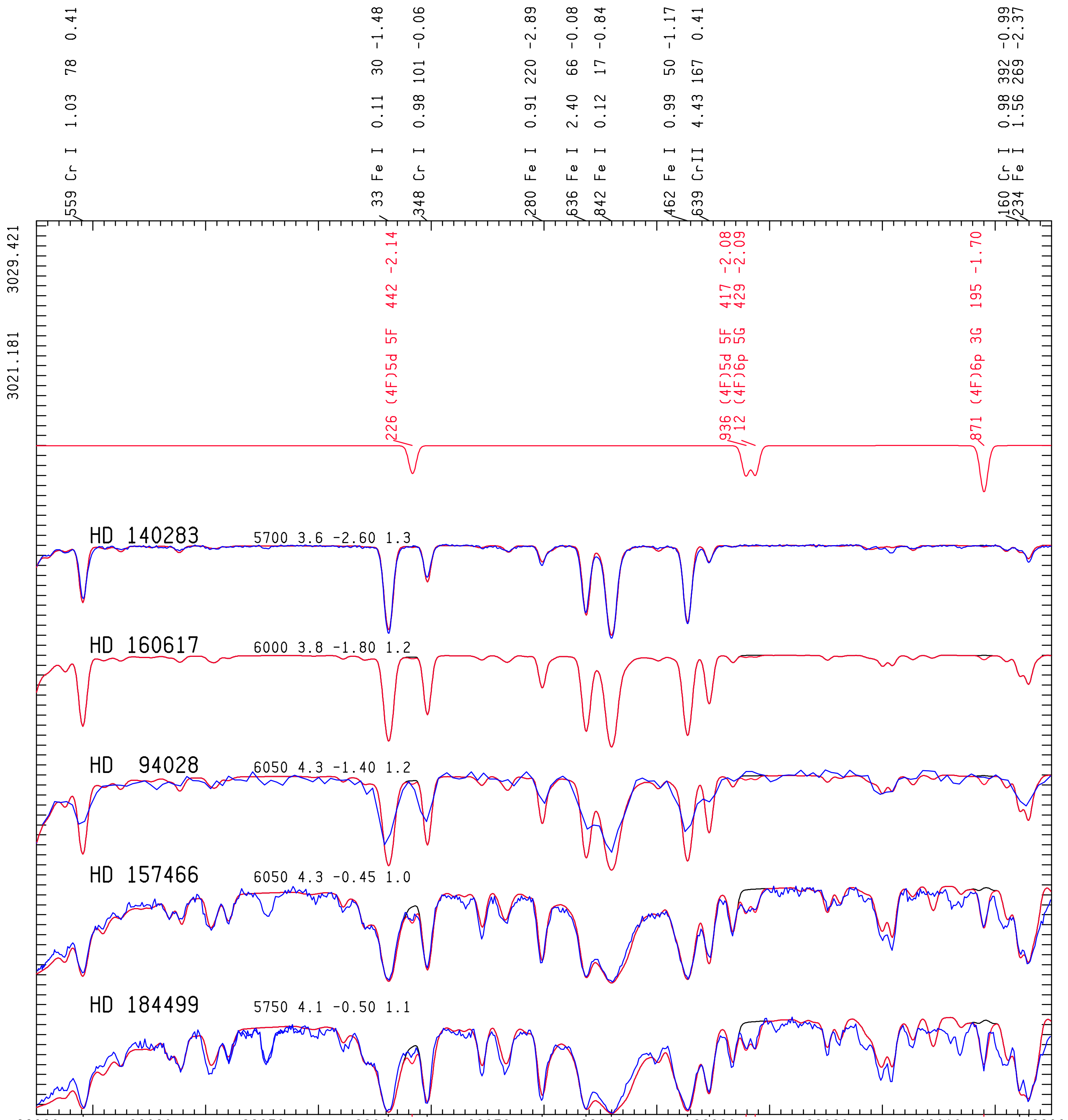

Figure 3. Comparisons like those in Figure 2 are shown for stars in the 3025 Å region.

weak lines that grow substantially below. Nonetheless, none of the four new identifications is strong enough to be detected in that spectrum, nor are any seen in the lower-resolution STIS E230M spectrum of HD 94028. Two new weak lines are seen in the stronger-lined, ground-based spectra of Figure 4. The star HD 184499 at the bottom of Figure 3 is now found at the top of Figure 4, and spectra of the Sun, the super-metal-rich giant μ Leo, and the metal-poor giant Arcturus appear at the bottom. The other two stars are a solar-metallicity dwarf and a metal-rich turnoff star. Figure 5 shows one new detection in the near-IR region near 8770 Å. Weak-lined stars are dropped, and the cool giant α Tau is substituted for μ Leo due to the excellent quality of its spectrum (Lebzelter et al. 2012).

In each figure the new identifications stand out: the red line is deeper than the black. The calculated and observed positions of the four 5.0 (4F)6p 3G lines all coincide, confirming our result for its energy value. Each newly identified line is well reproduced in all stars. Moreover, the strengths of the new lines match regardless of stellar temperature. The two reddest 5.0 (4F)6p 3G lines illustrate this well. The line at 4480.82 Å in Figure 4 is stronger in Arcturus than in the Sun, but the line at 8772.53 Å in Figure 5 is stronger in the Sun than in Arcturus.

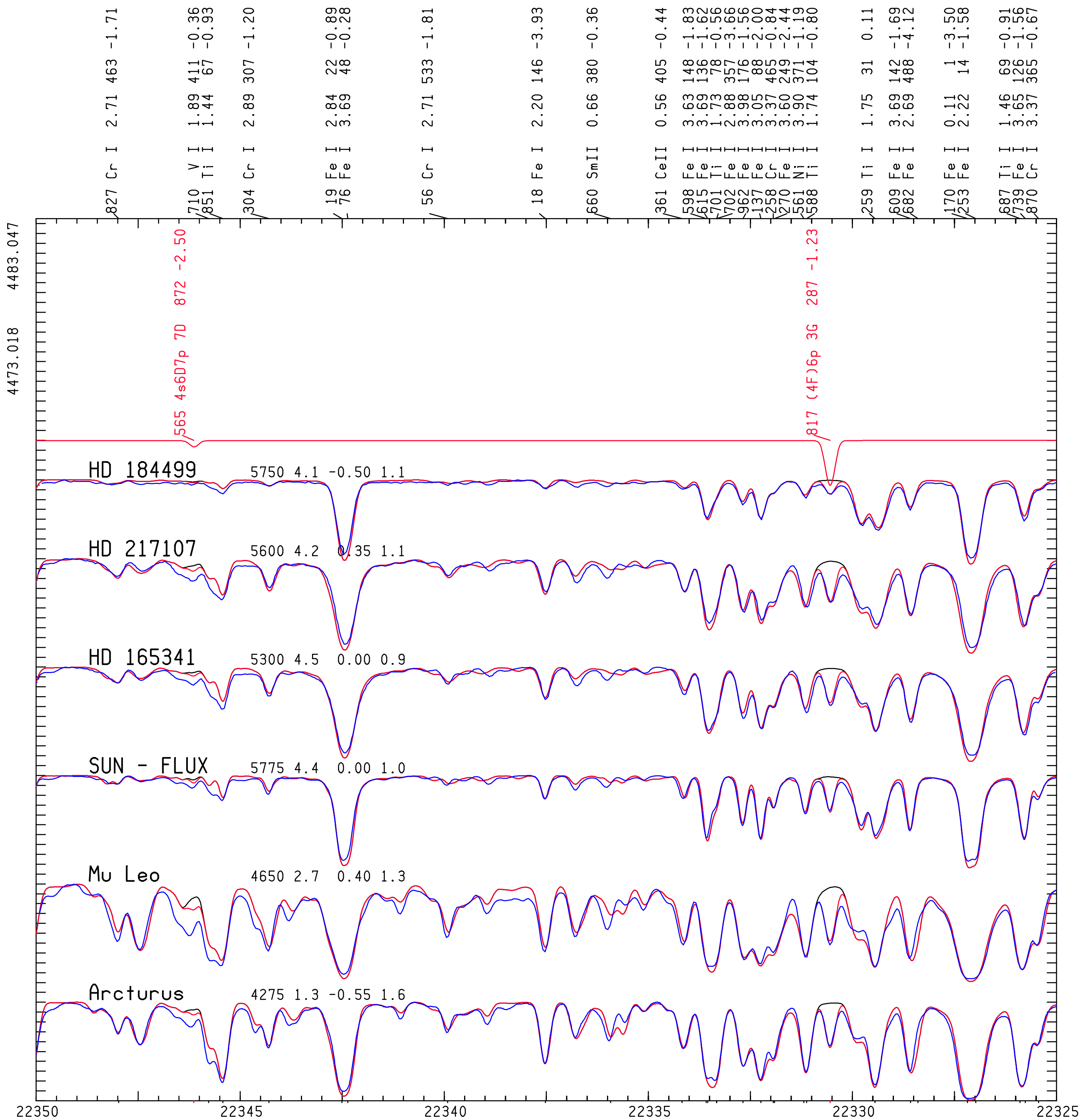

Figure 4. Comparisons like those in Figure 2 are shown for five stars in the 4480 Å region.

The former has a value of 37045.93 cm^{-1} for its lower excitation potential, while the latter has a high value of 47960.94 cm^{-1}. Taken together, the figures also illustrate the general trend for both known and unidentified lines to become weaker toward the red.

7. RESULTS TO DATE

In this way, we have now matched four or more transitions in 66 levels with energies up to 67716 cm^{-1}. In so doing, we have identified more than 2000 individual lines over 1600 Å–5.4 μm that are strong enough to be detected in warm and cool stars of moderate to high metallicity, of which more than a third are in the infrared. There are 1414 lines from 2000 Å to 9000 Å with log $gf > -3$, and 154 lines blueward to 1680 Å with log $gf > -4$. From 9000 Å to 5.4 μm are over 700 lines with log $gf > -2$. The transitions whose energies are most easily established are those with strong lines in well-observed, uncrowded regions (e.g., Figures 2 and 4). These form the majority of the levels we have successfully identified to date.

Thanks to the UV spectra, and to the high quality of the solar and Arcturus optical spectra, this approach reaches higher Fe I energies than any previous work, reaching a maximum at 67716 cm^{-1}. Five levels have energies higher even than the Fe I ionization potential of 63737.7 cm^{-1} (Schoenfeld et al. 1995). Table 2 lists separately for the newly identified even

Table 2
New Fe I Levels and Energies

Expanded Label	Label	J	E (cm^{-1})	σ (cm^{-1})
23 Even Levels:				
3d6 4s(6D)4d e7F	4s6D4d e7F	0	51143.92	0.03
3d7(4F)4d 5D	(4F)4d 5D	0	54304.21	0.02
3d6 4s(6D)4d 5D	4s6D4d 5D	0	58428.17	0.03
3d6 4s(4D)4d 5P	4s4D4d 5P	1	58628.41	0.03
3d7(4P)5s 3P	(4P)5s 3P	1	59300.54	0.03
3d6 4s(4D)4d 3D	4s4D4d 3D	2	58779.59	0.02
3d7(4F)5d 5F	(4F)5d 5F	2	59366.79	0.02
3d6 4s(4D)4d 3P	4s4D4d 3P	2	60087.26	0.03
3d7(2F)4s 1F	(2F)4s 1F	3	38602.26	0.02
3d7(4F)5d 5P	(4F)5d 5P	3	58616.11	0.02
3d7(4F)5d 5F	(4F)5d 5F	3	59196.87	0.02
3d6 4s(4D)4d 3G	4s4D4d 3G	3	59294.38	0.02
3d7(4F)5d 5F5D3G	5d 5F5D3G	3	59636.36	0.02
3d7(2G)5s 3G	(2G)5s 3G	3	61724.84	0.01
3d6 4s(6D)6d 3 + [4 +]	s6d 3 + [4 +]	4	59532.97	0.02
3d7(2G)5s 3G	(2G)5s 3G	4	61340.46	0.01
3d7(2G)5s 1G	(2G)5s 1G	4	61935.47	0.01
3d6 4s(3H)5s 5H	4s3H5s 5H	4	64531.78	0.03
3d7(2G)5s 3G	(2G)5s 3G	5	61198.49	0.01
3d7(2H)5s 1H	(2H)5s 1H	5	66293.98	0.01
3d7(2G)4d 3I	(2G)4d 3I	5	67687.99	0.01
3d6 4s(3H)5s 5H	4s3H5s 5H	6	64300.51	0.02
3d7(2G)4d 1I	(2G)4d 1I	6	67716.75	0.01
43 Odd Levels:				
d7(4F)5p 5D	(4F)5p 5D	0	54720.67	0.02
d7(2P)4p 1S	(2P)4p 1S	0	55179.91	0.08
d6(3P)4s4p(3P) 1P	3Psp3P 1P	1	50675.08	0.05
d7(4F)6p 5D	(4F)6p 5D	1	59703.05	0.05
d6(5D)4s(4F)7p 5D	4s4F7p 5D	1	60169.33	0.03
d6(5D)4s(6D)7p 5F	4s6D7p 5F	1	60336.16	0.03
d7(2F)4p 3D	(2F)4p 3D	1	60375.65	0.03
d6(3F)4s4p(1P)	3Fsp1P 3D	1	61075.16	0.03
d6(3P)4s4p(1P)	3Psp1P 3P	1	61155.62	0.06
d6(5D)4s(6D)7p 5D	4s6D7p 5D	2	60237.81	0.02
d6(3P)4s4p(1P) 3P	3Psp1P 3P	2	60585.09	0.04
d7(4F)7p 5D	(4F)7p 5D	2	61866.45	0.05
d7(4F)6p 5F	(4F)6p 5F	3	59418.83	0.03
d7(4F)6p 5G5D3D	6p 5G5D3D	3	59503.40	0.04
d6(3P)4s4p(3P) 1F	3Dsp3P 1F	3	59794.85	0.03
d6(5D)4s(6D)7p 5D	4s6D7p 5D	3	59875.89	0.04
d7(4F)6p 3G	(4F)6p 3G	3	60013.27	0.05
d6(5D)4s(6D)7p 5F	4s6D7p 5F	3	60055.93	0.05
d7(4F)7p 3D	(4F)7p 3D	3	61351.66	0.06
d7(4F)7p 5D	(4F)7p 5D	3	61770.94	0.04
d7(4F)7p 3G	(4F)7p 3G	3	62016.99	0.10
d7(4F)7p 5G	(4F)7p 5G	3	62287.54	0.10
d7(4F)8p 3D3G3F	8p 3D3G3F	3	62509.75	0.04
d7(4F)6p 5D	(4F)6p 5D	4	58729.80	0.08
d6(5D)4s(6D)7p 7D	4s6D7p 7D	4	59317.86	0.04
d7(4F)6p 5G	(4F)6p 5G	4	59377.30	0.02
d6(5D)4s(6D)7p 5D	4s6D7p 5D	4	59496.62	0.05
d6(5D)4s(6D)7p 7F	4s6D7p 7F	4	59595.12	0.03
d7(4F)6p 3G	(4F)6p 3G	4	59731.29	0.05
d6(5D)4s(6D)7p 5F	4s6D7p 5F	4	59804.54	0.02
d7(4F)7p 3F	(4F)7p 3F	4	61113.38	0.05
d7(4F)7p 5D	(4F)7p 5D	4	61173.80	0.03
d7(4F)7p 3G	(4F)7p 3G	4	61648.30	0.08
d7(4F)7p 5F	(4F)7p 5F	4	61678.26	0.05
d7(4F)8p 3G5G5F	8p 3G5G5F	4	62683.77	0.05
d7(4F)6p 5F	(4F)6p 5F	5	58609.56	0.03
d7(4F)6p 5G	(4F)6p 5G	5	59021.31	0.06
d7(4F)6p 3G	(4F)6p 3G	5	59357.03	0.02
d7(4F)7p 3G	(4F)7p 3G	5	61140.62	0.08

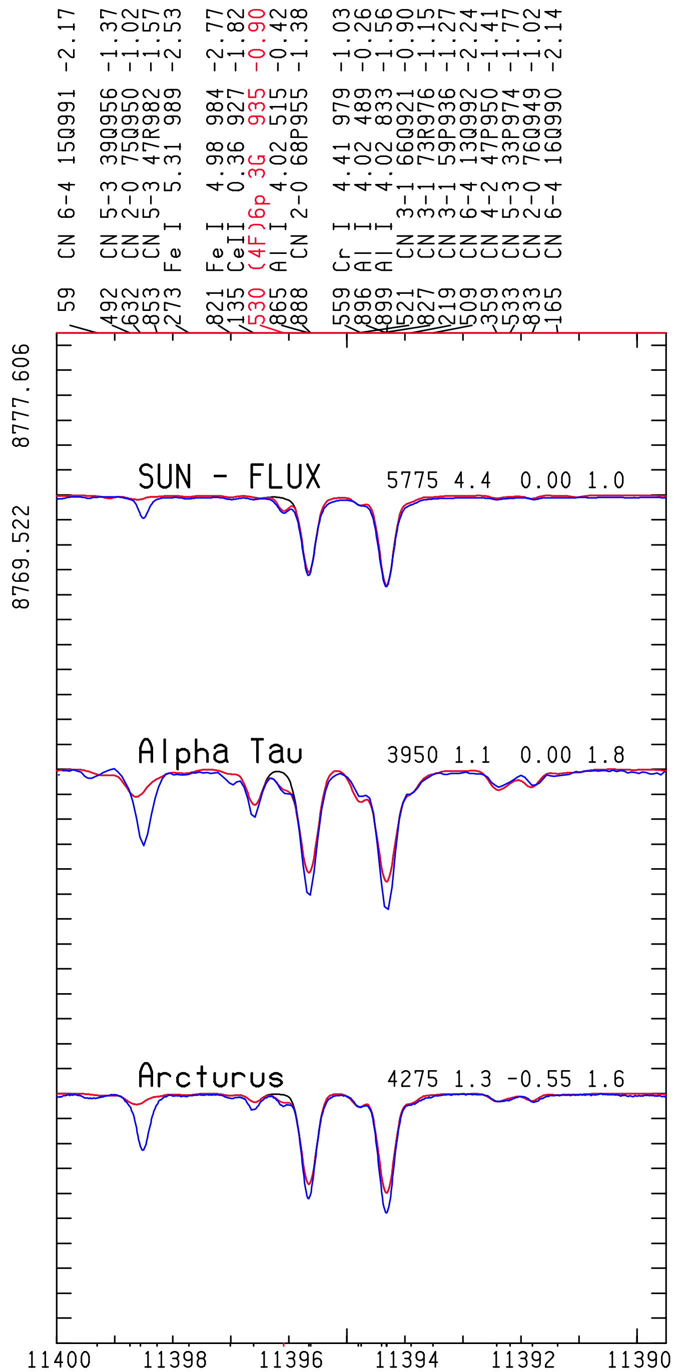

Figure 5. Comparisons like those in Figure 2 are shown for three stars in the 8770 Å region. The single newly identified Fe I line in this region appears at 8772.53 Å.

and odd levels the full and abbreviated labels and J value of each new level, and the associated energy and its uncertainty in wavenumbers.

Table 3 provides a wavelength-ordered list of the newly identified UV and optical lines. Wavelengths are given in vacuum below 2000 Å and in air above. For each line sufficiently strong and unblended, we estimate a *gf* value good to ±0.2 dex above 2617 Å. Blueward, *gf* value uncertainties rise to ±0.4 dex, as blends are poorly understood due to the lack of high-resolution spectra for stars with $-2 \leqslant$ [Fe/H] $\leqslant -1$ (Table 1). Even larger uncertainties apply in the 2150–2380 Å region, where HD 140283 is the only star with high-resolution spectra

Table 2
(continued)

Expanded Label	Label	J	E (cm^{-1})	σ (cm^{-1})
d7(4F)7p 5F	(4F)7p 5F	5	61155.95	0.05
d7(4F)7p 5G	(4F)7p 5G	5	61693.44	0.04
d6(3G)4s4p(1P) 3G	3Gsp1P 3G	5	62107.29	0.05

Notes. The three largest eigenvector components for each level can be found in the log files from the least squares fits, b2600e.log and b2600o.log, on the Kurucz Web site kurucz.harvard.edu/atoms/2600. All of the levels are mixed. The identification is a label, not a definitive assignment, especially for levels that are highly mixed.

(Table 1), and below 1950 Å, where line blending sharply increases and signal to noise drops (Peterson 2011). For every line for which the *gf* value can be assessed, Table 3 includes an entry for dgf, the log *gf* value from spectral matching minus the predicted log *gf* value. Table 3 also provides theoretical line damping constants. Γ_R is the logarithm of the radiative damping constant. Γ_S is the logarithm of the Stark damping constant/electron number density per cm^3. Γ_W is the logarithm of the van der Waals damping constant/neutral hydrogen number density per cm^3.

We have estimated the uncertainty in each individual energy determination from visual inspection of the goodness of fit of every reasonably unblended line. Our values range from 0.01 to 0.08 cm^{-1}, generally higher than the Nave & Johansson (1993a) uncertainty of 0.01 cm^{-1}. Since line profiles are broader at short wavelengths, as noted above, our uncertainties depend strongly on the distribution in wavelength of the subset of lines sufficiently unblended to constrain the energy.

Confirmation of our energy values is available for 41 levels of odd parity. These have two to five strong UV lines whose wavenumbers Brown et al. (1988) determined but could not classify. For many such lines they were able to assign an energy and J value; 31 of our 41 levels have these assignments, and our results always agree. The difference in the average of the 41 level energies between our work and theirs is 0.04 ± 0.03 cm^{-1}. The latter is similar to the 0.042 cm^{-1} rms value Schoenfeld et al. (1995) found in identifying infrared Fe I lines from the solar spectrum.

Our work also is uncovering individual line identifications of astrophysical interest. An example is the new Fe I identification at 6707.786 Å, a blend with the principal component of the Li I doublet at 6707.761 Å, upon which most stellar lithium abundance determinations depend. By analyzing the Ghezzi et al. (2009) high-quality bHROS spectrum of HD 217107, which has a very low lithium abundance, we were able to establish a *gf* value for this line. Its size is large enough to mildly affect the lithium abundances of solar-type stars of solar metallicity, and thus its presence is of importance for problems such as detecting lithium trends with stellar metallicity.

8. FUTURE PROSPECTS

Due to the very high data quality of the solar spectra, thousands of potentially detectable lines are available for many of the remaining unidentified levels, for levels of both even and odd parity. Over 2000 of these are in the infrared. From existing solar spectra we expect to identify hundreds more Fe I levels, and are beginning with new *f*, *g*, *h*, and *i* levels. In the UV, should additional spectra become available, hundreds of additional unknown Fe I levels could be found that have few strong lines outside the UV. These include levels with moderately weak lines scattered throughout the UV, and high-lying levels of odd parity with several strong lines below 1930 Å but few beyond.

Each set of new identifications is submitted for publication at the same time that Kurucz updates all the Fe I material on his website, including the new energy levels, line identifications, predicted *gf* values, and *gf* values derived from the stellar spectra. In this way, the entire community engaged in solving the astrophysical problems in Sections 1 and 2 is able to freely access and use these improvements immediately.

We thank Richard Monier for suggesting HD 72660 as a target and providing the far UV data, V. Smith and L. Ghezzi for providing the high-resolution HD 217107 Gemini-S spectrum, J. X. Prochaska for his reductions of the Keck HIRES

Table 3
Newly Classified Lines of Fe I

Wavelength (nm)	log *gf*	dgf	E_even (cm^{-1})	J_e	Label_e	E_odd (cm^{-1})	J_o	Label_o	Γ_R	Γ_S	Γ_W
160.5458	−3.197	...	0.000	4	4s2 a5D	62287.54	3	(4F)7p 5G	7.76	−3.71	−6.99
160.5966	−3.591	...	415.933	3	4s2 a5D	62683.77	4	8p 3G5G5F	8.30	−3.23	−7.02
161.0117	−2.672	...	0.000	4	4s2 a5D	62107.29	5	3Gsp1P 3G	8.32	−2.99	−7.03
161.0466	−3.777	...	415.933	3	4s2 a5D	62509.75	3	8p 3D3G3F	8.28	−3.80	−7.03
161.2461	−2.708	...	0.000	4	4s2 a5D	62016.99	3	(4F)7p 3G	8.12	−3.24	−7.09
161.6250	−2.065	...	415.933	3	4s2 a5D	62287.54	3	(4F)7p 5G	7.76	−3.71	−6.99
161.7973	−2.875	...	704.007	2	4s2 a5D	62509.75	3	8p 3D3G3F	8.28	−3.80	−7.03
161.8884	−2.605	...	0.000	4	4s2 a5D	61170.94	3	(4F) 7p 5D	7.39	−2.63	−6.96
162.0918	−2.814	...	0.000	4	4s2 a5D	61693.44	5	(4F) 7p 5G	7.69	−3.92	−7.08
162.1317	−1.956	...	0.000	4	4s2 a5D	61678.26	4	(4F)7p 5F	7.60	−3.47	−7.02
162.2105	−3.979	...	0.000	4	4s2 a5D	61648.30	4	(4F)7p 3G	7.95	−4.20	−7.12
162.3349	−2.683	...	415.933	3	4s2 a5D	62016.99	3	(4F)7p 3G	8.12	−3.24	−7.09
162.3811	−3.265	...	704.007	2	4s2 a5D	62287.54	3	(4F)7p 5G	7.76	−3.71	−6.99
162.7326	−3.827	...	415.933	3	4s2 a5D	61866.45	2	(4F)7p 3D	7.75	−3.45	−7.06
162.9859	−2.608	...	415.933	3	4s2 a5D	61170.94	3	(4F)7p 5D	7.39	−2.63	−6.96
163.2325	−2.719	...	415.933	3	4s2 a5D	61678.26	4	(4F)7p 5F	7.60	−3.47	−7.02
163.4687	−1.737	−0.60	0.000	4	4s2 a5D	61173.80	4	(4F)7p 5D	7.40	−3.66	−7.03
163.4990	−3.146	...	704.007	2	4s2 a5D	61866.45	2	(4F)7p 5D	7.70	−3.59	−7.06
163.5164	−1.975	−0.20	0.000	4	4s2 a5D	61155.95	5	(4F)7p 5F	7.10	−4.19	−7.06

(This table is available in its entirety in machine-readable form.)

data, and D. Silva and R. Hanuschik for the reduced UVES NGSL spectra. T. Ayres provided helpful information regarding STIS echelle dispersion solutions. We thank V. Hansteen for help with essential reference material, and the anonymous referee for a thorough and constructive review which improved the content and presentation of this paper. Support for this work under program number HST-AR-13263 was provided by NASA through a grant from the Space Telescope Science Institute, which is operated by the association of Universities for Research in Astronomy, Inc. under NASA contract NAS 5-26555. Ground-based spectra are largely based on observations made with ESO Telescopes at the Paranal Observatory with the UVES spectrograph under programs 065.L-0507(A), 072.B-0585(A), and 266.D-5655(A), and with the Keck Observatory HIRES spectrograph, under programs H6aH (PI: A. Boesgaard), N01H, N12H, and N13H (PI: D. Latham), U17H and U63H (PI: J. Prochaska), U35H (PI: A. Wolfe), and U44H (PI: M. Rich), as well as under programs GS-2066A-C-5 and GS-2006B-Q-47 at the Gemini Observatory, which is operated by the Association of Universities for Research in Astronomy, Inc., under cooperative agreement with the NSF on behalf of the Gemini partnership. This research has made use of the Keck Observatory Archive (KOA), which is operated by the W. M. Keck Observatory and the NASA Exoplanet Science Institute (NExScI), under contract with the National Aeronautics and Space Administration. Space-based spectra are based on observations made with the NASA/ESA *Hubble Space Telescope* under GO programs 7348, 7402, 8197, 9146, 9455, 9491, and 9804. These data were obtained from the *HST* and StarCat archives hosted by the Mikulski Archive for Space Telescopes (MAST). IRAF is distributed by the National Optical Astronomy Observatory, which is operated by the Association of Universities for Research in Astronomy, Inc., under cooperative agreement with the National Science Foundation.

REFERENCES

Ayres, T. R. 2010a, ApJS, 187, 149
Ayres, T. R. 2010b, in Ironing out the Wrinkles in STIS, 2010 STScI Calibration Workshop, ed. S. Deustua & C. Oliveira (STScI), 57 available at http://www.stsci.edu/institute/conference/cal10/proceedings
Bagnulo, S., Jehin, E., Ledoux, C., et al. 2003, ESO Msngr, 114, 10
Boesgaard, A. M., Rich, J. A., Levesque, E. M., & Bowler, B. P. 2011, ApJ, 743, 140
Brown, C. M., Ginter, M. L., Johansson, S., & Tilford, S. G. 1988, JOSA B, 5, 2125
Castelli, F., & Kurucz, R. L. 2003, in IAU Symp. 210, Modeling of Stellar Atmospheres, ed. N. Piskunov et al., CD-ROM poster A20; also astro-ph 0405087; ODFNEW models are available at http://kurucz.harvard.edu/grids/ and http://wwwuser.oats.inaf.it/castelli/grids.html
Castelli, F., & Kurucz, R. L. 2010, A&A, 520, 57
Chaffee, F. H., & Schroeder, D. J. 1976, ARA&A, 14, 23
Coelho, P. R. T. 2014, MNRAS, 440, 1027
Cowan, R. D. 1981, The Theory of Atomic Structure and Spectra, Los Alamos Series in Basic and Applied Sciences (Berkeley: Univ. California Press)
Dalcanton, J. J., Williams, B. F., Lang, D., et al. 2012, ApJS, 200, 18
Ghezzi, L, Cunha, K, Smith, V. V., et al. 2009, ApJ, 698, 451
Gregg, M. D., Silva, D., Rayner, J., et al. 2006, in The 2005 HST Calibration Workshop: Hubble After the Transition to Two-gyro Mode, ed. A. M. Koekemoer, P. Goudfrooij, & L. L. Dressel, 209, NASA/CP2006-214134, available at www.stsci.edu/institute/conference/ca105/workshop2005
Hinkle, K., Wallace, L., & Livingston, W. 1995, in Proc. Astronomical Society of the Pacific, Vol. 107, Infrared Atlas of the Arcturus Spectrum 0.9–5.3 μm, (San Francisco, CA: ASP), 1042
Hinkle, K., Wallace, L., Valenti, J., & Harmer, D. 2000, Visible and Near Infrared Atlas of the Arcturus Spectrum 3727–9300 Å (San Francisco, CA: ASP)
Johansson, S., Nave, G., Geller, M., et al. 1994, ApJ, 429, 419
Kelson, D. D., Williams, R. J., Dressler, A., et al. 2014, ApJ, 783, 110
Koleva, M., & Vazdekis, A. 2012, A&A, 538, 143
Kurucz, R. L. 1993, CD-ROM 18, SYNTHE Spectrum Synthesis Programs and Line Data (Cambridge: Smithsonian Astrophys. Obs.), available at http://kurucz.harvard.edu
Kurucz, R. L. 2005, Kitt Peak Solar Flux Atlas available at http://kurucz.harvard.edu/sun/fluxatlas2005
Kurucz, R. L. 2007, in The 9th Int. Colloq. Atomic Spectra and Oscillator Strengths (ASOS9), ed. G. M. Wahlgren, W. L. Wiese, & P. Beiersdorfer Phys.: Conf. Ser. J., 130
Kurucz, R. L. 2009, in AIP Conf. Ser., 1171, Recent Directions in Astrophysical Quantitative Spectroscopy and Radiation Hydrodynamics, ed. I. Hubeny, et al. (Melville, NY: AIP), 43
Kurucz, R. L. 2011, CaJPh, 89, 417
Lebzelter, T., Heiter, U., Abia, C., et al. 2012, A&A, 547, 108
Lind, K., Bergemann, M., & Asplund, M. 2012, MNRAS, 427, 50
Majewski, S. R., Wilson, J. C., Hearty, F., Schiavon, R. P., & Skrutskie, M. F. 2010, in IAU Symp. 265, ChemicalAbundances in the Universe: Connecting First Stars to Planets, ed. K. Cunha, M. Spite, & B. Barbuy (Cambridge: Cambridge Univ. Press), 480
Mashonkina, L., Gehren, T., Shi, J.-R., Korn, A. J., & Grupp, F. 2011, A&A, 528, A87
Nave, G., & Johansson, S. 1993a, A&A, 274, 961
Nave, G., & Johansson, S. 1993b, A&AS, 102, 269
Peterson, R. C. 2005, in Hubble 2005 Science Year in Review, ed. H. Ferguson (Baltimore, MD: NASA/STScI)
Peterson, R. C. 2008, in Space Telescope Sci. Inst. Newsletter, 25, no. 1 (Spring 2008; Baltimore, MD: NASA/STScI), 24
Peterson, R. C. 2011, ApJ, 742, 21
Peterson, R. C. 2013, ApJL, 768, L13
Peterson, R. C., Carney, B. W., Dorman, B., et al. 2002, in Proceedings of the NASA Laboratory Astrophysics Workshop, ed. F. Salama, 73
Peterson, R. C., Dalle Ore, C. M., & Kurucz, R. L. 1993, ApJ, 404, 333
Peterson, R. C., Dorman, B., & Rood, R. T. 2001, ApJ, 559, 372
Rodriguez-Merino, L. H., Chavez, M., Bertone, E., & Buzzoni, A. 2005, ApJ, 626, 411
Ruffoni, M. P., Allende Prieto, C., Nave, G., & Pickering, J. C. 2013, ApJ, 779, 17
Schoenfeld, W. G., Change, E. S., Geller, M., et al. 1995, A&A, 301, 583
Sneden, C., Cowan, J. J., & Gallino, R. 2008, ARA&A, 46, 241
Thorén, P., & Edvardsson, B. 2000, A&A, 363, L33
Tousey, R. 1988, JOSA B, 5, 2230
Vogt, S. S., Allen, S. L., Bigelow, B. C., et al. 1994, Proc. SPIE, 2198, 362